

# Efficient simulation of double-stranded DNA as a semiflexible polymer at full basepair resolution

Debabrata Panja

*Institute for Theoretical Physics, Universiteit Utrecht,  
Leuvenlaan 4, 3584 CE Utrecht, The Netherlands and  
Institute of Physics, Universiteit van Amsterdam, Science Park 904,  
Postbus 94485, 1090 GL Amsterdam, The Netherlands*

Gerard T. Barkema

*Institute for Theoretical Physics, Universiteit Utrecht,  
Leuvenlaan 4, 3584 CE Utrecht, The Netherlands and  
Instituut-Lorentz, Universiteit Leiden,  
Niels Bohrweg 2, 2333 CA Leiden, The Netherlands*

J.M.J. van Leeuwen

*Instituut-Lorentz, Universiteit Leiden,  
Niels Bohrweg 2, 2333 CA Leiden, The Netherlands*

## Abstract

Using a recently developed bead-spring model for semiflexible polymers, we develop an efficient algorithm to simulate double-stranded DNA (dsDNA) dynamics at full basepair resolution in the absence of hydrodynamic interactions. Polymer dynamics in the model is described by the Langevin equation. The model has four parameters. All of them are determined by matching to experimental data: the parameter  $d$  sets the distance between the consecutive beads, the two further parameters  $T^*$  and  $\nu$  in the Hamiltonian are chosen to match the experimental force-extension curve of dsDNA, while the Langevin friction coefficient  $\xi$  for the dynamics is determined by matching to the diffusion coefficient of small dsDNA segments in water at room temperature. We consider the persistence length of dsDNA to be  $\approx 37.7$  nm that corresponds to 114 beads in the model. The key to efficiency is the use of the dynamical properties of the polymer's fluctuation modes in the algorithm, as opposed to the use of simply the physical positions of the beads. We show that, at full basepair resolution, within an accuracy tolerance level of 5% of several key observables, the model allows for single Langevin time steps of  $\approx 1.6, 8, 16$  and  $32$  ps for a dsDNA model-chain consisting of 64, 128, 256 and 512 basepairs (i.e., chains of 0.55, 1.11, 2.24 and 4.48 persistence lengths) respectively. Correspondingly, in one hour, a standard desktop computer can simulate 0.23, 0.56, 0.56 and 0.26 ms of these dsDNA chains respectively. We compare our results to those obtained from other methods, and demonstrate the use of the present method by simulating efficiently the tumbling behavior of a dsDNA segment in a shear flow, at full basepair resolution.

PACS numbers: 36.20.-r, 64.70.km, 82.35.Lr

## I. INTRODUCTION

Over the last decades, there has been a surge in research activities in the physical properties of biopolymers, such as double-stranded DNA (dsDNA), filamental actin (F-actin) and microtubules. Semiflexibility is a common feature they share: they preserve mechanical rigidity over a range, characterized by the persistence length  $l_p$ , along their contour. (E.g., for a dsDNA, F-actin and microtubules,  $l_p \approx 40$  nm [1, 2],  $\sim 16\mu\text{m}$  [3] and  $\sim 5$  mm [4] respectively.) Generally speaking, the stretching modulus for semiflexible polymers is far greater than their bending modulus, i.e., the chains are effectively inextensible at the length for which the persistence length is relevant.

For theoretical understanding of the properties of semiflexible polymers it is often convenient to ignore the monomeric building blocks, and to instead describe the chain conformation by an inextensible and continuous differentiable curve. The resulting model is known as the Kratky-Porod wormlike chain (WLC) model [5]. The WLC model, its subsequent modifications [6–9], and recent analyses [10–15] have been very successful in describing static/mechanical properties of dsDNA, such as its force-extension curve and the radial distribution function of its end-to-end distance.

It is however not trivial to study polymer dynamics using the WLC model. The contour length of the polymer is constrained in the WLC model, and Lagrangian multipliers of a varying degree of sophistication need to be implemented in order to enforce a contour length that is either strictly fixed [16–20], or fixed on average [21, 22]. In any case, computer simulations require a discrete set of coordinates, so working with variations of the WLC on a computer requires discretization of the WLC chain conformation.

If a discretization needs to be performed anyway in order to simulate a semiflexible polymer on the computer, the following question arises: why not simulate the polymer in its full glory of monomers, e.g., individual basepairs for a dsDNA? Precisely from this perspective, recently two of us introduced a bead-spring model for semiflexible polymers [23], where each bead corresponds to a single constituting monomer. The model has four parameters. All of them are determined from experimental data. One parameter,  $d$ , sets the distance between the consecutive beads. Two further parameters,  $T^*$  and  $\nu$ , in the Hamiltonian are determined by matching to the experimental force-extension curves (see next paragraph for the fourth parameter). The mechanical and dynamical properties of this

bead-spring model were subsequently studied [23, 24], and were found to faithfully reproduce the well-known features of semiflexible polymers.

In this paper, we put this model on the computer to simulate semiflexible polymer dynamics, focusing on dsDNA at full basepair resolution. We use Langevin dynamics, for which each basepair, represented by a bead in the model, is subjected to a random thermal force and a drag force. There is no hydrodynamic interactions among the beads. This is in fact not a problem when it comes to comparing to experimental results for dsDNA segments up to a few persistence lengths, since at these lengths a semiflexible polymer does not form a coil, and therefore should be free-draining. Indeed, this is the feature that allows us to meaningfully compare the diffusion coefficients of short model dsDNA segments to those from experiments, from which we determine the fourth (and the last) parameter of the model,  $\xi$ , which describes the Langevin friction on the beads.

The conventional simulation approach would be to integrate the corresponding Langevin equations of motion in time, with a simple integration scheme such as the Euler method. This is however, not efficient. Instead, we use the behavior of the polymer’s fluctuation modes in this model [24], and use these modes to achieve 2-3 orders of magnitude longer time steps for integrating the Langevin equations forward in time — this is the main achievement of this paper.

The basic idea of using the polymer’s fluctuation modes in order to simulate its dynamics originates from the Rouse model [25], in which the equations of motion can be integrated with an arbitrarily large time step. This is effected by the fact that the dynamical eigenmodes in the Rouse model are known exactly, and therefore they evolve in time independently of each other. Unfortunately, for semiflexible polymers one cannot identify the set of independent modes, so the time-evolution cannot be simulated with arbitrarily large time-steps as one can in the case of a Rouse chain. However, we show that one *can* construct modes that are to a large degree independent, which is the key to achieving a large time-step for time-integration at full monomeric (basepair in the present case) resolution. As we simulate the dsDNA at various chain lengths, we track three observables as a function of the size of the time-step: the end-to-end vector autocorrelation function, the middle bond vector autocorrelation function, and the mean-square displacement of the middle bead wrt the center-of-mass of the chain. The accuracy tolerance level of 5% of these three observables determine  $\Delta t_{\text{max}}$ , the maximum size of the time-step, and is summarized below in Table I.

chain length (bp)	$\Delta t_{\max}$ (ps)	$t_{\max}$ (ms)
64	1.59	0.23
128	7.96	0.56
256	15.9	0.56
512	15.9	0.26

TABLE I: The maximum size of the integration time-step  $\Delta t_{\max}$  for various chain lengths for dsDNA. The persistence length we use is  $l_p \approx 37.6$  nm [2], corresponding to  $\approx 114$  basepairs. Also noted in the last column is the amount of real time  $t_{\max}$  our model can simulate on a standard linux desktop computer in one hour.

On the one hand, with increasing polymer length at some point the algorithm will definitely not be useful, as the time required to simulate the dynamics will be prohibitively long. In these cases, e.g., when one deals with dsDNA of genome sizes (a few to tens of kbps), it is more useful to work with a coarse-grained description, wherein a single bead represents several basepairs. On the other, simulating a chain significantly shorter than the persistence length poses no problem, as then one can consider the chain configuration to be a small perturbation from that of a straight rod. It is the middle range (i.e., the chain lengths are of the order of the persistence length, when the chain configuration deviates significantly from that of a straight rod) that is not easy to simulate — our work is meant to fill this void.

We stress that use of the polymer’s fluctuation modes should be equally valid for other types of semiflexible polymers. In yet broader perspective, bridging the time gap between the microscopic time of particle vibrations and the macroscopic times of interest is a key problem which shows up in many areas of physics. We envisage that the use of the system’s fluctuation modes, instead of the use of individual particles’ motions, in such systems will open up new possibilities to achieve large time-steps in computer simulations.

This paper is organized as follows. In Sec. II we briefly introduce the model, and identify the parameter values of the model Hamiltonian for dsDNA at full basepair resolution. In Sec. III we describe the equations for polymer dynamics. Section IV is devoted to the time-integrated algorithm for the equation of motion for the polymer in mode representation. In Sec. V we test the time-integration algorithm for dsDNA, while in Sec. VI we elaborate on

our numerical results presented in Table I. We conclude the paper with a discussion in Sec. VII, including a comparison with the time-steps achieved in the existing literature. Finally, in the ancillary files we present a movie of a tumbling dsDNA segment in a shear flow, generated by using this algorithm, to illustrate the usefulness of the simulation approach.

## II. THE MODEL

The model we use for semiflexible polymers is described in detail in Ref. [23]. The Hamiltonian for the model is of the form

$$\mathcal{H} = \frac{\lambda}{2} \sum_{n=1}^N (|\mathbf{u}_n| - d)^2 - \kappa \sum_{n=1}^{N-1} \mathbf{u}_n \cdot \mathbf{u}_{n+1}. \quad (1)$$

Here  $\mathbf{u}_n = \mathbf{r}_n - \mathbf{r}_{n-1}$  is the bond vector between bead  $n-1$  and  $n$ , with  $\mathbf{r}_n$  being the position of the  $n$ -th bead ( $n = 0, 1, \dots, N$ ). The first term in this Hamiltonian relates to the longitudinal stiffness of the chain, while the second term relates to its resistance to bending. The parameters in the Hamiltonian are the following. The quantity  $d$  sets the length scale of a bond — if only the first term would be present, bonds would assume the length  $d$ . The presence of the second term in the Hamiltonian causes an elongation of the bonds such that the average bond length is  $a = bd$ , with a factor  $b$  that depends on the type of the polymer. Further,  $\lambda$  and  $\kappa$  are two parameters, relating to the longitudinal (stretching) and transverse (bending) stiffness of the chain. In order to have  $\mathcal{H}$  represent semiflexible polymers, both parameters  $\lambda$  and  $\kappa$  typically will have to be large. Instead of working in terms of  $\lambda$  and  $\kappa$ , we choose the ratios  $\nu = \kappa/\lambda$  and  $T^* = k_B T / (\lambda d^2)$  as characteristic parameters to describe the model [23], which reduces the Hamiltonian to

$$\frac{\mathcal{H}}{k_B T} = \frac{1}{2T^*} \left[ \sum_{n=1}^N (|\mathbf{u}_n| - 1)^2 - 2\nu \sum_{n=1}^{N-1} \mathbf{u}_n \cdot \mathbf{u}_{n+1} \right]. \quad (2)$$

Note that stability of the Hamiltonian requires  $0 < \nu < 1/2$ , and that in these variables [23, 24]

$$b = \frac{1}{1 - 2\nu}. \quad (3)$$

### A. The model parameters for dsDNA at full basepair resolution

For dsDNA at full basepair resolution, the physical distance between the beads equals  $a = 0.33$  nm, the length of a basepair. The two parameters  $T^*$  and  $\nu$  can be chosen by matching the force-extension curve for the polymer, leading to  $\nu = 0.35$  and  $T^* = 0.034$  [23]. Following Eq.(3), the factor  $b$  then turns out to be  $\approx 3.3$ , so that the length parameter  $d \approx 0.1$  nm. At full basepair resolution the number of beads  $(N + 1)$  simply equals the number of basepairs present in the dsDNA chain.

The equilibrium and the dynamical properties of the model, specially in relation to the well-known properties of semiflexible polymers have been studied in detail in Refs. [23, 24]. Nevertheless, in order to demonstrate the usability of this model for reaching long length and time-scales on a computer we need to revisit the dynamical equations resulting from the Hamiltonian (2).

## III. POLYMER DYNAMICS

We describe the polymer dynamics in terms of the Langevin equation. It is natural to choose the positions of the beads as the dynamical variables, obeying the equations

$$\frac{d\mathbf{r}_n(t)}{dt} = -\frac{1}{\xi} \frac{\partial \mathcal{H}}{\partial \mathbf{r}_n} + \mathbf{g}_n(t). \quad (4)$$

Here  $\xi$  is the friction coefficient and  $\mathbf{g}_n$  is the Gaussian distributed random thermal force on bead  $n$  due to the solvent molecules, with the fluctuation spectrum

$$\langle g_m^\alpha(t) g_n^\beta(t') \rangle = \frac{2k_B T}{\xi} \delta^{\alpha,\beta} \delta_{m,n} \delta(t - t'). \quad (5)$$

For numerical evaluation of these equations it is useful to reduce time and distances to dimensionless variables. We therefore scale distances and time by  $d$  and time by  $\xi/\lambda$ , i.e., we write the bead positions as  $\mathbf{r}_n = \mathbf{r}'_n d$  and  $t = \xi\tau/\lambda$ , which gives the Langevin equation the form

$$\frac{d\mathbf{r}'_n(t)}{d\tau} = -\frac{\partial \mathcal{H}'}{\partial \mathbf{r}'_n} + \mathbf{g}'_n(\tau). \quad (6)$$

Correspondingly, the dimensionless random force

$$\mathbf{g}'_n = \frac{\mathbf{g}_n d}{\lambda} \quad (7)$$

has the correlation function

$$\langle g_m'^\alpha(\tau) g_n'^\beta(\tau') \rangle = 2T^* \delta^{\alpha,\beta} \delta_{m,n} \delta(\tau - \tau'). \quad (8)$$

In order to restore notational simplicity henceforth we omit the primes on the variables.

### A. The dynamical equations in terms of polymer's fluctuation modes

It is of course possible to simulate polymer dynamics using Eqs. (6-8), with the bead positions as variables. This however only allows Langevin time step  $\Delta\tau = 0.1$ , and at  $\Delta\tau_{\max} \approx 0.3$  the integration scheme even becomes unstable. An equivalent manner to simulate polymer dynamics is to use its fluctuation modes as variables. The main advantage of the latter is that the modes with longer length-scales have slower decay times, and as result one can make a separation in time scales, which in turn allows for the possibility of larger time steps, i.e., faster simulations that eventually achieves 2-3 orders of magnitude larger integration time steps. In this section we describe the method.

As for describing polymer dynamics in terms of the polymer's fluctuation modes (described by the mode variables  $\mathbf{R}_p$ ), note that any transformation of the type

$$\begin{cases} \mathbf{R}_p = \sum_n \mathbf{r}_n \phi_{n,p}, \\ \mathbf{r}_n = \sum_p \phi_{n,p} \mathbf{R}_p, \end{cases} \quad (9)$$

where  $\phi_{n,p}$  is an orthogonal matrix, satisfying

$$\sum_p \phi_{m,p} \phi_{n,p} = \delta_{mn}, \quad (10)$$

leaves the dynamical equation (6) form invariant; i.e.,

$$\frac{d\mathbf{R}_p(t)}{d\tau} = -\frac{\partial\mathcal{H}}{\partial\mathbf{R}_p} + \mathbf{G}_p. \quad (11)$$

Here  $\mathbf{G}_p$  is the transform of  $\mathbf{g}_n$ :

$$\mathbf{G}_p = \sum_n \mathbf{g}_n \phi_{n,p}, \quad (12)$$

whereas the derivative with respect to  $\mathbf{R}_p$  can be calculated with the chain rule

$$\frac{\partial\mathcal{H}}{\partial\mathbf{R}_p} = \sum_n \frac{\partial\mathcal{H}}{\partial\mathbf{r}_n} \phi_{n,p}. \quad (13)$$



Returning to our Hamiltonian (2), we see that it can be rewritten in the form [23]

$$\frac{\mathcal{H}}{k_B T} - N/2 = \frac{1}{2} \sum_{m,n} \mathbf{r}_m \cdot H_{m,n} \mathbf{r}_n - L_c = \mathcal{H}^* - L_c, \quad (14)$$

with  $L_c$  the contour length

$$L_c = \sum_n u_n. \quad (15)$$

In this form of the Hamiltonian, the  $\mathcal{H}^*$  term is not only quadratic in the bead positions, but also  $H_{mn}$  becomes diagonal under the transformation ( $p = 0, 1, \dots, N-1$ ) [23]

$$\phi_{n,p} = \left( \frac{2}{N+1} \right)^{1/2} \cos \left( \frac{p(n+1/2)\pi}{N+1} \right), \quad (16)$$

which are of the same form as the Rouse modes for a flexible polymer [25], with eigenvalues

$$\zeta_p^l = 2 \left[ 1 - \cos \left( \frac{p\pi}{N+1} \right) \right] \left[ 1 - 2\nu \cos \left( \frac{p\pi}{N+1} \right) \right]. \quad (17)$$

In other words,  $\mathcal{H}^*$  is simply expressed as

$$\mathcal{H}^* = \frac{1}{2} \sum_p \zeta_p^l R_p^2. \quad (18)$$

Unfortunately though, the term  $L_c$  in the Hamiltonian (14) is not diagonal in the Rouse mode representation, meaning that  $L_c$  contains coupling among different Rouse modes. Consequently, the equation of motion for the polymer takes the form

$$\frac{d\mathbf{R}_p(t)}{d\tau} = -\zeta_p^l \mathbf{R}_p + \mathbf{H}_p + \mathbf{G}_p, \quad (19)$$

where  $\mathbf{H}_p = -\partial L_c / \partial \mathbf{R}_p$ . In this form it becomes clear that the times scales for the modes, given by  $(\zeta_p^l)^{-1}$ , vary widely with the mode index  $p$ , ranging from large for small  $p$  to small for  $p$  of the order  $N$ . In the next sections, by separating the time-scales in this manner, that the important physics is contained in the low modes and that treating them correctly opens up a window of opportunity to take large time steps in the numerical integration of Eq. (11).

Having said the above, we also note that the choice of the Rouse modes in representing the dynamical equation is by no means unique. An equivalent representation in terms of the polymer's fluctuation modes, well-elaborated in one of our own publications [24] is as follows. In terms of the bead positions  $\mathbf{r}_n$  of the chain one can expand the Hamiltonian

around its ground state, which has a configuration of a straight rod. The second term in this expansion, involving the Hessian  $\partial^2 \mathcal{H} / \partial \mathbf{r}_m \partial \mathbf{r}_n$ , is also quadratic in the bead positions, but it includes not only  $\mathcal{H}^*$ , but also some contribution from  $L_c$ . Indeed, as shown in Ref. [24], the corresponding modes then yield the well-known transverse (bending) and longitudinal (stretching) modes of a semiflexible chain, with eigenvalues  $\zeta_p^t$  and  $\zeta_p^l$  respectively. [Of these, the longitudinal modes are identical to the Rouse modes (16-17), which explains our choice of notation for the eigenvalue in Eq. (17).] Thus, an equivalent, and perhaps more natural, choice of representing the dynamical equation (11) would be to use the longitudinal and the transverse modes. Our experience, however, is that using the Rouse mode representation makes the code faster and more robust for parameters  $T^*$  and  $\nu$  typical for dsDNA, to which we stick to in the rest of this paper (and also in our earlier publication [24]).

#### IV. TIME-INTEGRATED ALGORITHM FOR THE EQUATION OF MOTION FOR THE POLYMER IN MODE REPRESENTATION

We start with the (obvious) statement that without the coupling term  $\mathbf{H}_p$ , the integration of the equations (19) is straightforward. Each mode develops as an Ornstein-Uhlenbeck process, which admits an exact solution. As this is the basis of our refinements of the algorithm, we illustrate our method of time-integration of the equation of motion for the polymer by considering one scalar mode  $R(t)$  with decay coefficient  $\zeta$ , a coupling force  $H(t)$  and random force  $G(t)$ . It is useful to first make the substitution (c.f. the interaction representation in quantum mechanics)

$$R(t) = \exp(-\zeta t) \tilde{R}(t), \quad (20)$$

leading to the equation for  $\tilde{R}(t)$

$$\frac{d\tilde{R}(t)}{dt} = [H(t) + G(t)] \exp(\zeta t). \quad (21)$$

Integrating this equation over a finite time interval  $\Delta t$  and multiplying the result with  $\exp(-\zeta \Delta t)$  then yields

$$R(t + \Delta t) = \exp(-\zeta \Delta t) R(t) + \overline{H}(t) + \overline{G}(t), \quad (22)$$

where  $\overline{G}$  is given by

$$\overline{G}(t) = \int_0^{\Delta t} dt' \exp[\zeta(t' - \Delta t)] G(t + t'), \quad (23)$$

and likewise,  $\overline{H}$  is given by

$$\overline{H}(t) = \int_0^{\Delta t} dt' \exp[\zeta(t' - \Delta t)] H(t + t'). \quad (24)$$

The distribution of  $\overline{G}(t)$  is, as an integral (sum) over independent Gaussian random variables, i.e., a Gaussian random variable with variance

$$w^2(\Delta t) = T^*[1 - \exp(-2\zeta\Delta t)]/\zeta; \quad (25)$$

i.e., in formula (23) the distribution reads

$$P(\overline{G}) = \frac{1}{\sqrt{\pi}w(\Delta t)} \exp\left(-\frac{\overline{G}^2}{2w^2(\Delta t)}\right). \quad (26)$$

Note here that Equation (22) is an exact substitute for the Langevin equation with an arbitrary time step.

From the above one sees that the use of the polymer's fluctuation modes to time-integrate the equation of motion has two aspects:

- (i) If we manage to make  $H$  small, we may treat the modes to be evolving independently, with only a small perturbation due to the coupling.
- (ii) We need to find an expression for the integral  $\overline{H}(t)$ , while we only have an expression for the initial value  $H(t)$ .

Clearly, the more successful we are with point (i), the less severe point (ii) becomes.

### A. A more functional form of $\mathbf{H}_p$ for polymer dynamics

The expression for  $\mathbf{H}_p$  follows from Eqs. (14) and (17)

$$\mathbf{H}_p = \frac{\partial L_c}{\partial \mathbf{R}_p} = \sum_n \frac{\partial L_c}{\partial \mathbf{r}_n} \phi_{n,p} = \sum_n [\hat{\mathbf{u}}_n - \hat{\mathbf{u}}_{n+1}] \phi_{n,p}, \quad (27)$$

where  $\hat{\mathbf{u}}_n = \mathbf{u}_n/u_n$ , is the unit bond vector, and  $u_n = |\mathbf{u}_n|$ . By rearranging the summation variable  $n$  we write

$$\mathbf{H}_p = \sum_{n=1}^N \hat{\mathbf{u}}_n \chi_{n,p}, \quad (28)$$

with

$$\chi_{n,p} = \phi_{n,p} - \phi_{n-1,p} = 2 \left( \frac{2}{N+1} \right)^{1/2} \sin \left( \frac{p\pi}{2(N+1)} \right) \sin \left( \frac{pn\pi}{N+1} \right). \quad (29)$$

Using the bond-length factor  $b$  introduced in (3), it is natural to write

$$\hat{\mathbf{u}}_n = \mathbf{u}_n/b + \Delta\hat{\mathbf{u}}_n = (1 - 2\nu)\mathbf{u}_n + \Delta\hat{\mathbf{u}}_n. \quad (30)$$

Inherent to Eq. (30) is the build-up of the following approximation scheme, as we demonstrate below. In the limit of small  $T^*$  (i.e., high  $\lambda$ ) — e.g.,  $T^* = 0.034$  for dsDNA — the chain does not stretch much, hence we expect  $\Delta\hat{\mathbf{u}}_n$  to be much smaller than  $\mathbf{u}_n/b$ ; in other words, setting  $\Delta\hat{\mathbf{u}}_n$  to zero provides a rather good approximation for  $\hat{\mathbf{u}}_n$ . Further, since  $\mathbf{u}_n$  can be expressed as

$$\mathbf{u}_n = \sum_{q=1}^N \chi_{n,q} \mathbf{R}_q, \quad (31)$$

with

$$\sum_{n=1}^N \chi_{n,p} \chi_{n,q} = \left[ 2 \sin \left( \frac{p\pi}{2(N+1)} \right) \right]^2 \delta_{p,q}, \quad (32)$$

we can write

$$\mathbf{H}_p = (1 - 2\nu) \left[ 2 \sin \left( \frac{p\pi}{2(N+1)} \right) \right]^2 \mathbf{R}_p + \Delta\mathbf{H}_p, \quad (33)$$

where  $\Delta\mathbf{H}_p$  is simply given by

$$\Delta\mathbf{H}_p = \sum_{n=1}^N \chi_{n,p} \mathbf{u}_n [1/u_n - (1 - 2\nu)]. \quad (34)$$

The first term of (33) can be combined with  $-\zeta_p^l \mathbf{R}_p$  in Eq. (19), leading to the combination

$$\zeta_p = \zeta_p^l - (1 - 2\nu) \left[ 2 \sin \left( \frac{p\pi}{2(N+1)} \right) \right]^2, \quad (35)$$

which curiously enough is a reasonably good approximation of the eigenvalue  $\zeta_p^t$  for the  $p$ -th transverse mode [24]. This allows us to rewrite Eq. (19) as

$$\frac{d\mathbf{R}_p(t)}{d\tau} = -\zeta_p \mathbf{R}_p + \Delta\mathbf{H}_p + \mathbf{G}_p, \quad (36)$$

with the hope that  $\Delta\mathbf{H}_p$  remains small in comparison to the full term  $\mathbf{H}_p$ . We will test this in Sec. IV B.

We note that the dynamical equation (36) is still an exact representation of the Langevin equation (4).

## B. Time-integration of $\Delta\mathbf{H}_p$

Following the notation of Eq. (24) we now discuss an approximation for

$$\overline{\Delta\mathbf{H}_p(\tau)} = \int_0^{\Delta\tau} dt' \exp[\zeta_p^l(t' - \Delta\tau)] \Delta\mathbf{H}_p(t + t'). \quad (37)$$

In any time-forward integration process we clearly know the initial value of the integrand in (37). We assume that the integrand will decay in the interval  $\Delta\tau$  with an exponent comparable to the decay of the modes around  $p$ , as the strongest correlation exists between nearby modes [24]. A further assumption we make here is that since  $\Delta\mathbf{H}_p$  contains purely the bond-length fluctuations, which are part of the longitudinal fluctuations of the chain, we expect the exponent to be equal to  $\zeta_p^l$ ; leading us to the approximation

$$\Delta\mathbf{H}_p(\tau + \tau') \simeq \Delta\mathbf{H}_p(\tau) \exp(-\zeta_p^l \tau'). \quad (38)$$

Then the integral (24) simply reduces to

$$\overline{\Delta\mathbf{H}_p(\tau)} \simeq \Delta\mathbf{H}_p(\tau) \frac{\exp(-\zeta_p \Delta\tau) - \exp(-\zeta_p^l \Delta\tau)}{\zeta_p^l - \zeta_p}. \quad (39)$$

For modes where  $\zeta_p \Delta\tau$  and  $\zeta_p^l \Delta\tau$  are both small, the expression reduces to

$$\overline{\Delta\mathbf{H}_p(\tau)} \simeq \Delta\mathbf{H}_p(\tau) \Delta\tau, \quad p \text{ small}. \quad (40)$$

Indeed, this is precisely what one would expect for the modes that do not decay in the interval  $\Delta\tau$ . Similarly, for the modes where  $\zeta_p^l \Delta\tau$  is large one gets

$$\overline{\Delta\mathbf{H}_p(\tau)} \simeq \Delta\mathbf{H}_p(\tau) \frac{\exp(-\zeta_p \Delta\tau)}{\zeta_p^l - \zeta_p}, \quad (41)$$

i.e. an exponentially small contribution. In other words, the form (38) gives a smooth suppression of the coupling between the high- $p$  modes, depending on the choice of  $\Delta\tau$ . For time steps  $\Delta\tau$  in which the high modes are equilibrated, we treat them as independent modes. In the extreme limit of very large  $\Delta\tau$  all the modes become independent. That limit clearly misses the important non-linear effects between the modes, which essentially puts a limit on how large  $\Delta\tau$  we can get away with.

## V. TESTING THE TIME-INTEGRATION ALGORITHM FOR dsDNA AT FULL BASEPAIR RESOLUTION

Having explained the time-integration algorithm in the previous section in general terms within this bead-spring model, we now set out to test it on a single dsDNA chain at full basepair resolution. However, before we do so, it is imperative to us that we check whether Eq. (36) provides a reasonable time-integration scheme. That starts with a comparison of the  $\mathbf{H}_p$  and  $\Delta\mathbf{H}_p$  terms in Eq. (36).

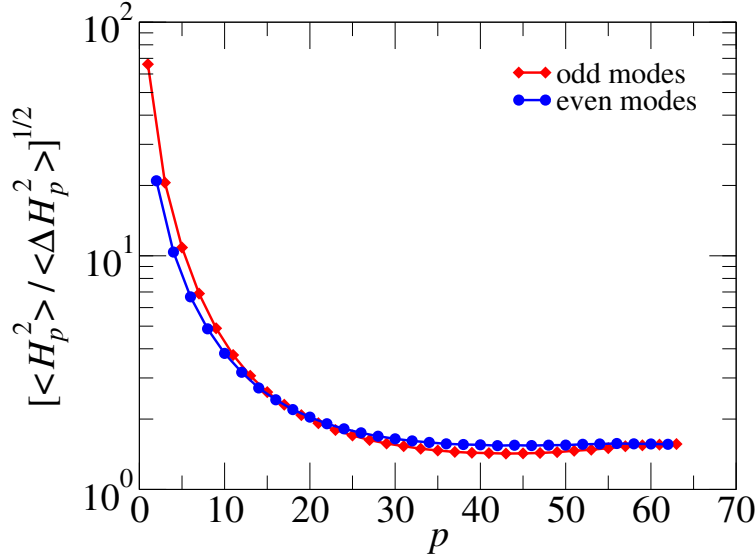


FIG. 1: The ratio  $[\langle H_p^2 \rangle / \langle \Delta H_p^2 \rangle]^{1/2}$  for a dsDNA chain of length  $N = 63$ .

### A. Comparing $\mathbf{H}_p$ and $\Delta\mathbf{H}_p$ for dsDNA at full basepair resolution

Both  $\mathbf{H}_p$  and  $\Delta\mathbf{H}_p$  are fluctuating quantities, so a proper comparison between them would be to plot the ratio of  $[\langle H_p^2 \rangle / \langle \Delta H_p^2 \rangle]^{1/2}$  as a function of  $p$ . In doing so we note that odd- $p$  modes are even under reversal of renumbering the beads from  $n$  to  $N - n$  and even- $p$  modes are odd under this reversal. Since the ground state is even under this reversal, it means that the odd- $p$  modes are excited more by thermal fluctuations. We therefore plot this ratio separately for the even and the odd modes in Fig. 1 for a dsDNA with  $N = 63$ , i.e., a dsDNA chain 64 basepairs long. The plot shows the approximation scheme (33) in action — for low  $p$ -values, i.e., modes corresponding to large length-scales, the remainder  $\Delta\mathbf{H}_p$  is only

a fraction of  $\mathbf{H}_p^{(0)}$ . This opens up a systematic way of dealing with  $\Delta\mathbf{H}_p$  that still couples the different (Rouse) modes, which we exploit in the next subsection.

### B. Testing the vulnerability of the algorithm to enlarging $\Delta\tau$ for dsDNA at full basepair resolution

As already pointed in Sec. IV A, with the approximations (38-41) we cannot limitlessly increase  $\Delta\tau$ . We now test numerically on dsDNA how far we can go on with increasing  $\Delta\tau$  for  $N = 63, 127, 255$  and  $511$ . In other words, we obtain the values of  $\Delta\tau_{\max}$  for these values of  $N$ . The quantities we track, collectively denoted by  $Q(t)$ , in order to determine  $\Delta\tau_{\max}$  are the autocorrelation functions in time of (i) the end-to-end vector and (ii) the middle bond, and (iii) the mean-square displacement (msd) of the middle bead wrt the position of the center-of-mass of the chain. Our test procedures are divided into two groups: the equilibrium values for these quantities, collectively denoted as  $Q(0)$  and their dynamical behavior. The test procedure is as follows.

In the first group, we determine the quantities (i-iii) for several values of  $\Delta\tau$ , namely (a)  $N = 63$  :  $\Delta\tau = 0.1, 0.2, 0.5, 1, 2, 5, 10, 20, 50$  and  $100$ , (b)  $N = 127$  :  $\Delta\tau = 1, 2, 5, 10, 20, 50, 100, 200, 500$  and  $1000$ , (c)  $N = 255$  :  $\Delta\tau = 1, 2, 5, 10, 20, 50, 100, 200, 500, 1000, 2000, 5000$  and  $10000$ , (d)  $N = 511$  :  $\Delta\tau = 5, 10, 20, 50, 100, 200, 500, 1000, 2000, 5000, 10000, 20000$  and  $50000$ . The data are averaged over 13 realizations of run length  $\tau = 8 \times 10^7$  for  $N = 63$ ,  $\tau = 8 \times 10^8$  million for  $N = 127$ ,  $\tau = 8 \times 10^9$  for  $N = 255$  and  $\tau = 4 \times 10^{10}$  for  $N = 511$  for each realization. In the first group of tests we determine their equilibrium values as a function of  $\Delta\tau$ . As benchmarks of these equilibrium quantities we also perform Monte Carlo (MC) simulations, which are carried out again by using the mode representation, permitting one to take large MC steps in the slow modes and small steps in the fast modes. We accept the runs as valid if all measured observables deviate at most 5% from their MC values, the other ones we reject as invalid, leading to a set of  $\Delta\tau_{\max}$  values for each  $N$ .

The procedure is demonstrated in Fig. 2. We scale the equilibrium values by the corresponding MC ones, which means that the  $y$ -values of the rescaled equilibrium quantities should lie between 0.95 and 1.05, indicated by the yellow band representing our acceptance threshold. The highest  $\Delta\tau$  values, for which all the equilibrium quantities — taking into

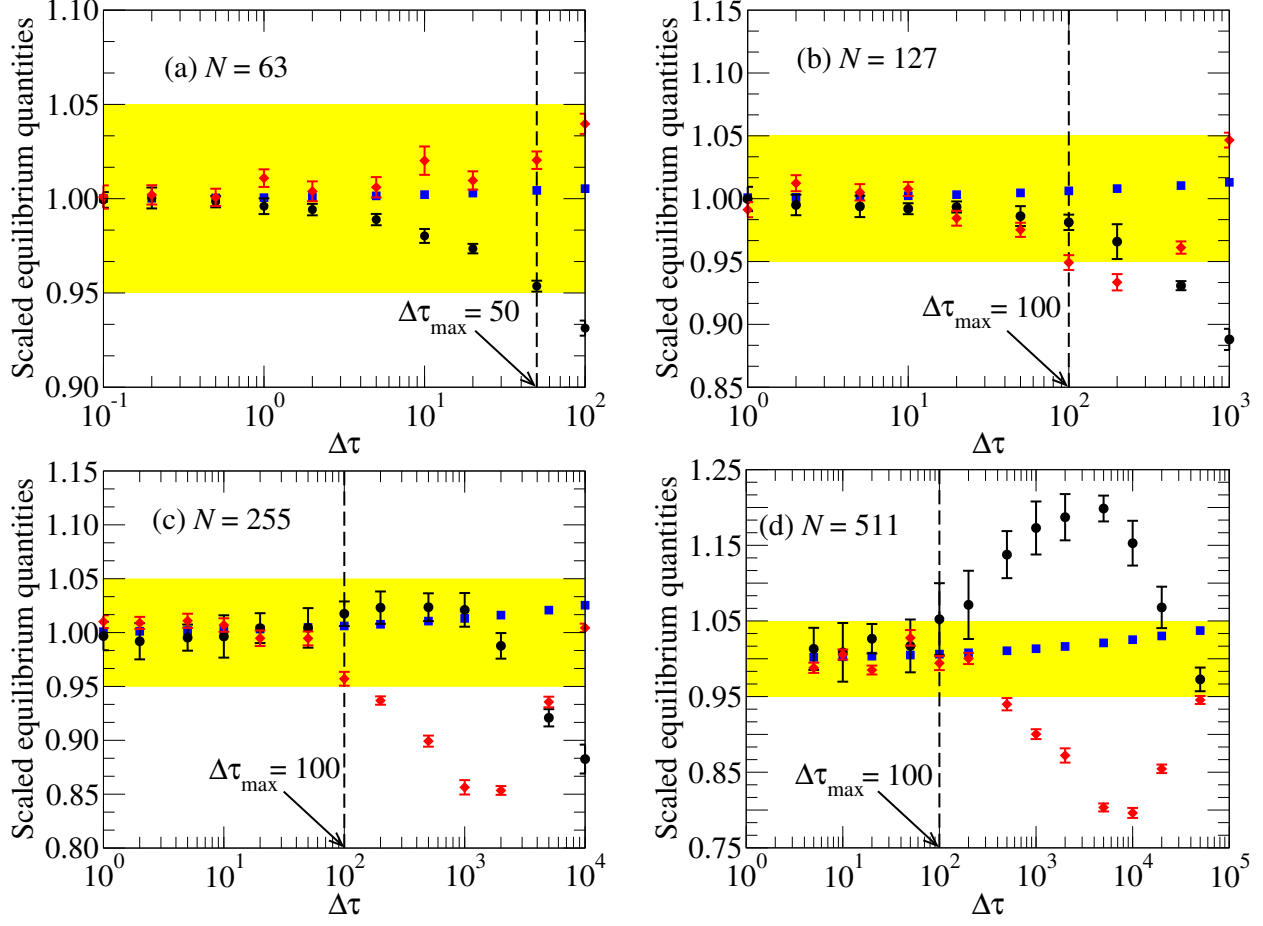


FIG. 2: Determination of  $\Delta\tau_{\max}$  from the equilibrium values  $Q(0)$ . The autocorrelation functions in time of the end-to-end vector are shown in black circles, the middle bond in blue squares, and the mean-square displacement (msd) of the middle bead wrt the position of the center-of-mass of the chain in red diamonds. The data are rescaled by their MC values: (a)  $N = 63$ , (b)  $N = 127$ , (c)  $N = 255$  and (d)  $N = 511$ . The error bars for the autocorrelation functions in time of the middle bond are not shown since they are smaller than the symbol size. The yellow band represents 5% validity thresholds. See text for details.

consideration the error bars — fall within the yellow band gets us the  $\Delta\tau_{\max}$  values for each  $N$  for the first group of test.

In the second group of tests we use time-dependent quantities  $Q(t)$ . In this case MC simulations are of no help, so we treat the lowest value of  $\Delta\tau$  for each  $N$  as the benchmark. Let us describe the procedure for  $N = 63$ , for which the lowest value of  $\Delta\tau$  equals  $\Delta\tau_{\min} = 0.1$ . We choose a few fixed values of the time  $\tau$ , such as  $\tau = 100, 1000, 10000$  and  $100000$ ; first



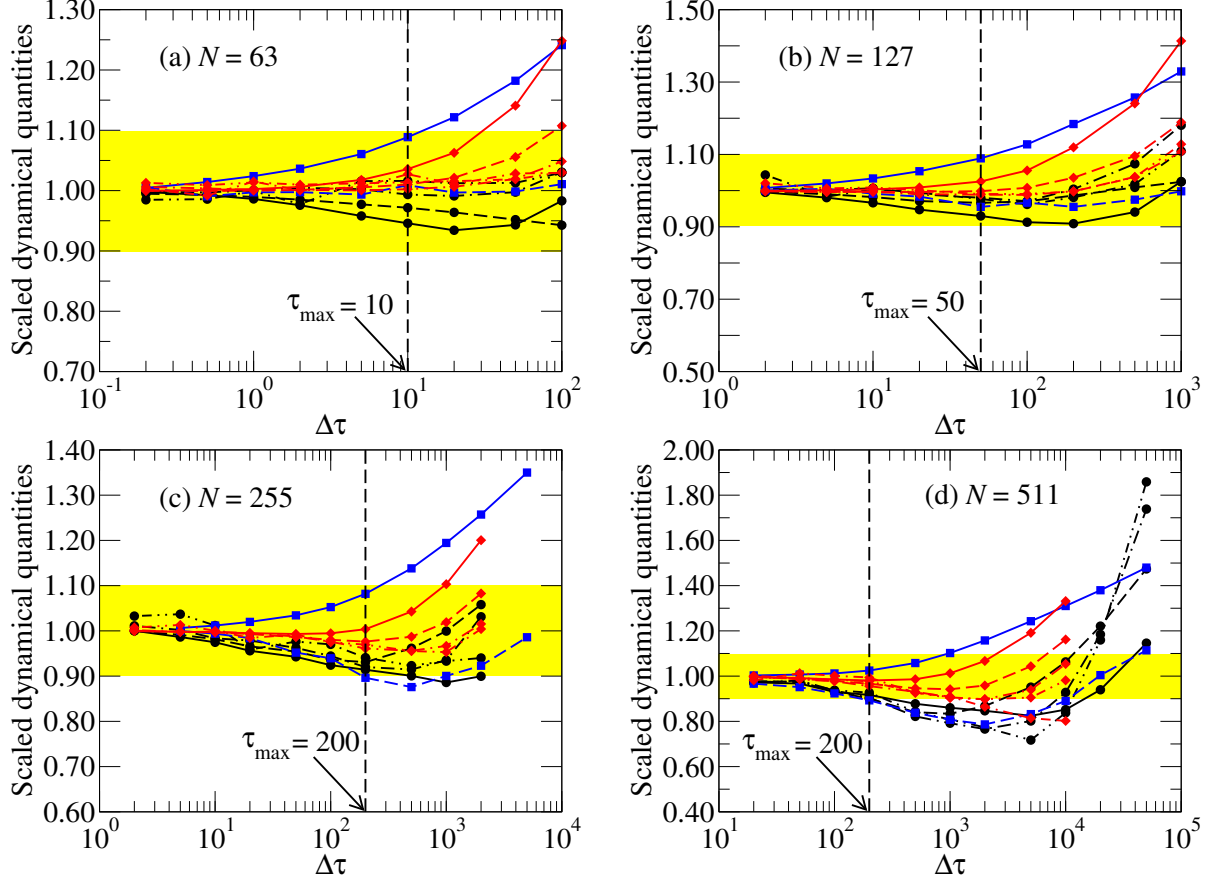


FIG. 3: Determination of  $\Delta\tau_{\max}$  from  $Q(t)$ . The autocorrelation functions in time of the end-to-end vector are shown in black circles, the middle bond in blue squares, and the mean-square displacement (msd) of the middle bead wrt the position of the center-of-mass of the chain in red diamonds. The data are rescaled by  $\tilde{Q}(\Delta\tau_{\min})$ . (a)  $N = 63$  ( $\Delta\tau_{\min} = 0.1$ ):  $\tau = 100$  (solid line), 1000 (long-dashed), 10000 (dashed-dot-dashed), 100000 (dashed-dot-dot-dashed); (b)  $N = 127$ , ( $\Delta\tau_{\min} = 1$ ):  $\tau = 1000$  (solid line), 10000 (long-dashed), 100000 (dashed-dot-dashed), 1000000 (dashed-dot-dot-dashed); (c)  $N = 255$  ( $\Delta\tau_{\min} = 1$ ):  $\tau = 10000$  (solid line), 100000 (long-dashed), 1000000 (dashed-dot-dashed), 10000000 (dashed-dot-dot-dashed) and (d)  $N = 511$  ( $\Delta\tau_{\min} = 5$ ):  $\tau = 100000$  (solid line), 1000000 (long-dashed), 10000000 (dashed-dot-dashed), 100000000 (dashed-dot-dot-dashed). The yellow band represents 10% validity thresholds. See text for details.

obtain the quantities  $Q(\tau)$  and numerically differentiated quantity  $dQ(\tau)/d\tau$  for all values of  $\Delta\tau$ , and thereafter the effective decay constant for  $Q(\tau)$ , i.e., ratio  $\tilde{Q}(\tau) = \frac{1}{Q(\tau)} \frac{dQ(\tau)}{d\tau}$ . [Clearly, for a given value of  $\tau$ ,  $\tilde{Q}(\tau)$  is also a function of  $\Delta\tau$ , i.e.,  $\tilde{Q}(\tau) \equiv \tilde{Q}(\tau, \Delta\tau)$ .] We

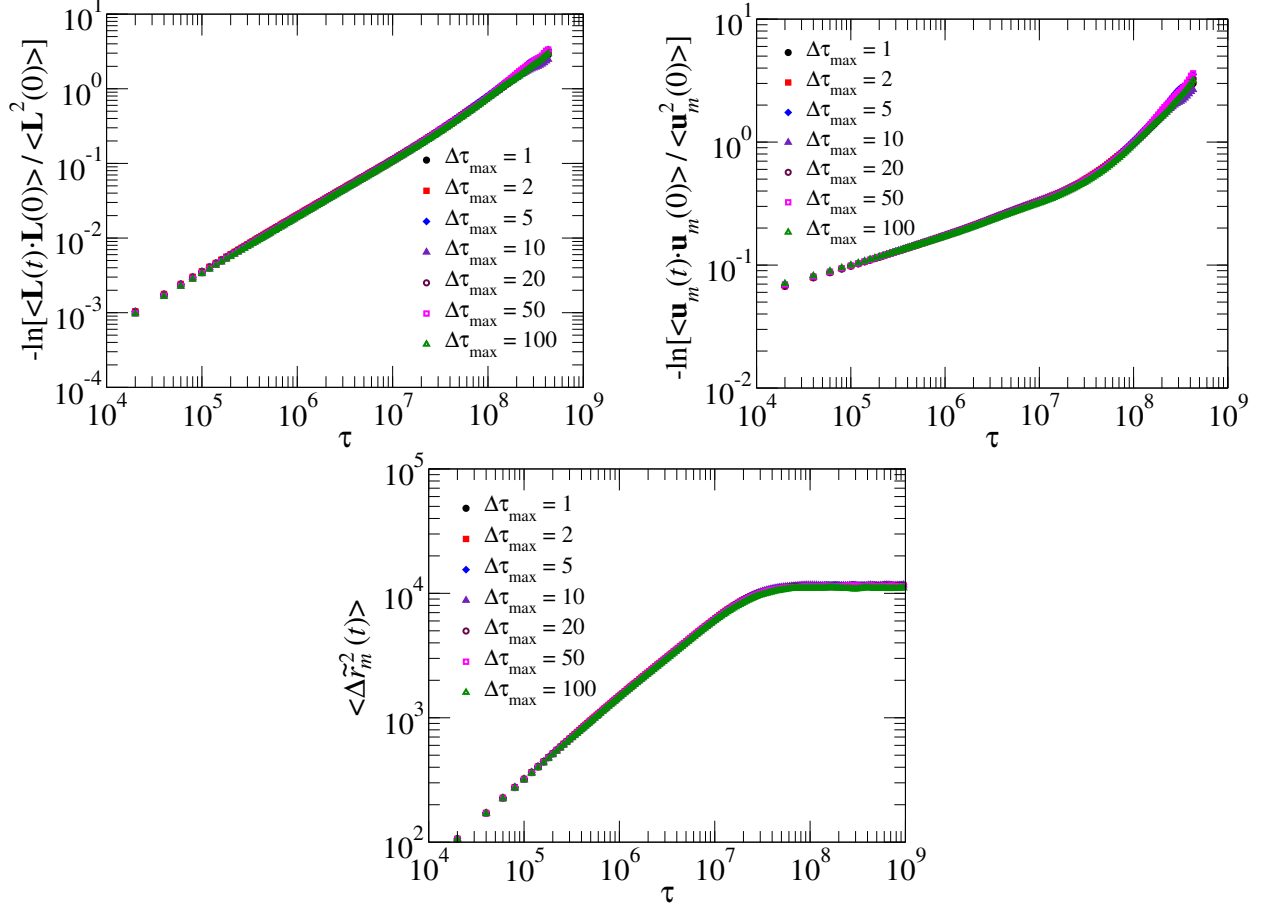


FIG. 4: The  $Q(t)$  curves for  $\Delta\tau = \Delta\tau_{\min}$  to  $\Delta\tau_{\max}$  for  $N = 255$ : the normalized autocorrelation function of the end-to-end vector  $\mathbf{L}$  and the middle bond vector  $\mathbf{u}_m$ , and the means-square displacement  $\langle \Delta \tilde{r}_m^2(t) \rangle$  of the middle bead measured wrt the center-of-mass of the chain. The data for all values of  $\Delta\tau$  as it should be — the figure demonstrates the validity of our procedure.

then demand that at these values of  $\tau$  the ratio  $\tilde{Q}(\Delta\tau)/\tilde{Q}(\Delta\tau_{\min})$  does not deviate from unity by more than 10%. The 10% is chosen by the following criterion: the statistical errors in the quantities  $Q(t)$  are typically of order 2%, which accumulate to  $\sim 4\%$  for  $\tilde{Q}(t)$ , to which we need to add our 5% criterion as explained above, and further round their sum off to 10%. (The larger tolerance for the dynamical variables is a consequence of a lack of clean benchmark data, which was provided by MC simulations for equilibrium observables.) The result of this procedure is presented in Fig. 3 — note that this (numerical) procedure is prone to noise more than it has been for the first group that involved  $Q(0)$ , so we only carry out the procedure for which the procedure is not spoiled by noise in the data.

The results from the two figures 2-3 are summarized in Table II. The final value of  $\Delta\tau_{\max}$  for any given value of  $N$  is clearly the smaller one emerging from the two groups. Said differently, use of the final values of  $\Delta\tau_{\max}$  (as it appears in Table II) in simulations means that the data for  $Q(t)$  should not differ from each other by more than 5% at any time. As an example of the validity of our procedure, we plot the  $Q(t)$  curves for  $N = 255$  in Fig. 4 — for all  $\Delta\tau$  values between  $\Delta\tau_{\min}$  and  $\Delta\tau_{\max}$  the curves are on top of each other as they should be.

$N$	$\Delta\tau_{\max}$ from equilibrium quantities $Q(0)$	$\Delta\tau_{\max}$ from dynamical quantities $Q(t)$	final $\Delta\tau_{\max}$ min[columns 2 and 3]
63	50	10	10
127	100	50	50
255	100	200	100
511	100	200	100

TABLE II: List of  $\Delta\tau_{\max}$  values for the values of  $N$  studied in this paper for dsDNA at full basepair resolution.

## VI. TRANSLATING $\Delta\tau_{\max}$ TO REAL TIMES

We now translate  $\Delta\tau_{\max}$  to real times using the experimental parameters characteristic for dsDNA.

To this end we note that in Langevin dynamics there are no hydrodynamic interactions among the beads, leading to the center-of-mass diffusion of a single chain  $D = k_B T / (N\xi)$ . In experiments hydrodynamic interactions are always present, however, they only become important when the chain is long enough to exhibit self-avoiding walk statistics. Thus, as long as the chains are substantially smaller than the persistence length, they behave essentially as straight rods, for which hydrodynamic interactions among beads are not important. In other words, for chains substantially smaller than the persistence length we can meaningfully compare the center-of-mass diffusion coefficient resulting from our model and experiments. This comparison then yields us the correspondence of  $\Delta\tau_{\max}$  to real times.

The diffusion coefficient of small dsDNA segments has been studied using various techniques, such as capillary electrophoresis [29, 30], dynamic light scattering [31], NMR [32], and fluorescent recovery after photobleaching [33]. Of these, the first three converge on the value  $\approx 1.07 \times 10^8 \text{ nm}^2/\text{s}$  for a 20 bp dsDNA in water at room temperature (23° C), while the last one reports  $5.3 \times 10^7 \text{ nm}^2/\text{s}$  for 21 bp dsDNA. We decide to stick to the values reported by the first three because of the consistency among different experimental methods, and upon equating  $D = k_B T / (N\xi)$  to  $\approx 1.07 \times 10^8 \text{ nm}^2/\text{s}$  for  $N = 20$ , with  $k_B T = 4.089 \text{ pN nm}$  at 23° C, we obtain

$$\xi = 1.91 \times 10^{-12} \text{ kg/s.} \quad (42)$$

Further, writing the relation  $t = \xi\tau/\lambda$  [see Sec. II, and the paragraph above Eq. (6)], in terms of the parameters  $T^*$  and  $\nu$ , the conversion between the real time  $t$  and the dimensionless time  $\tau$  is obtained as

$$t = \frac{T^*}{b^2} \frac{a^2 \xi}{k_B T} \tau. \quad (43)$$

The combination  $a^2 \xi / (k_B T)$  is with  $a = 0.33 \text{ nm}$  and the value of  $\xi$  from Eq. (42) equal to

$$\frac{a^2 \xi}{k_B T} = 52.0 \text{ ps.} \quad (44)$$

Inserting the dsDNA values one gets

$$t \equiv c\tau, \quad \text{with} \quad c = 0.16 \text{ ps.} \quad (45)$$

*i.e. one unit of dimensionless time corresponds to 0.16 ps of real time.*

With the above information we can now translate  $\Delta\tau_{\text{max}}$ , the maximum time step at full basepair resolution, to real times  $\Delta t_{\text{max}}$  in Table III. Also noted in the last column of Table III is the amount of real time  $t_{\text{max}}$  our model can simulate in an hour on a standard linux desktop computer at full basepair resolution.

## VII. DISCUSSION

Using a recently developed bead-spring model, in the absence of hydrodynamic interactions among the beads, in this paper we have developed an efficient algorithm to simulate the dynamics of dsDNA as a semiflexible polymer at full basepair resolution. Polymer dynamics

chain length (bp)	$\Delta\tau_{\max}$	$\Delta t_{\max}$ (ps)	$t_{\max}$ (ms)
64	10	1.59	0.23
128	50	7.96	0.56
256	100	15.9	0.56
512	100	15.9	0.25

TABLE III: Time forward integration steps  $\Delta t_{\max}$  in real times for various chain lengths at full basepair resolution. Also noted in the last column the amount of real time  $t_{\max}$  our model can simulate on a standard linux desktop computer in one hour.

in the model is described by the Langevin equation. We consider dsDNA at persistence length  $l_p \approx 37.7$  nm that corresponds to 114 beads in the model. The model has four parameters. All of them are determined by matching to experimental data. We show that, within an accuracy tolerance level of 5% of several key observables, the model allows for large single Langevin time steps; as summarized in Table III.

The key to such large time-steps is to use the polymer’s fluctuation modes as opposed to the individual beads for simulating the dynamics. The conventional simulation approach would be to integrate the corresponding Langevin equations of motion in time, with a simple integration scheme such as the Euler method. This is however, not an efficient method, as one can get to  $\Delta\tau_{\max}$  to  $\approx 0.1$ ; at  $\Delta\tau_{\max} \approx 0.3$  the integration algorithm even becomes unstable. Instead, we use the polymer’s fluctuation modes to integrate the dynamical equations forward in time. Although any choice of orthogonal basis functions can be used to describe the polymer’s fluctuation modes, we found that the choice of the Rouse modes provides the most stable and robust results. Use of the Rouse modes allows us to take 2 to 3 orders of magnitude longer time steps for integrating the Langevin equations forward in time, as evidenced in Table III.

In a broader perspective, bridging the time gap between the microscopic time of particle vibrations and the macroscopic times of interest, is a key problem which shows up in many areas of physics. We envisage that the use of the system’s fluctuation modes, instead of the use of individual particles’ motions, in such systems will open up new possibilities to achieve large time-steps in computer simulations.

We remark that the numbers in the table are only indicative for the order of magnitude of the allowable time step for various reasons. First of all, the choice 5% for the equilibrium quantities (consistently, 10% for the dynamical quantities) is arbitrary. Secondly, the percentage error in the physical observables depends on the quantity chosen. We find that in most cases the msd of the middle monomer decides the size of  $\Delta\tau_{\max}$ . The end-to-end vector also plays that role in a few cases, while the middle bond is not at all critical. For the accuracy percentage (of course) it also matters whether one takes e.g. the square of the end-to-end vector (as we did) or the vector itself (the latter choice halves the error). Finally, the maximum allowable time step depends also on the parameters  $T^*$  and  $\nu$ . We found that the dependence on  $T^*$  is rather weak but the sensitivity to the value of  $\nu$  is much stronger. Nevertheless, despite these reservations, the gain of 2 to 3 orders of magnitude stands firm.

Large time steps can also be obtained by coarse graining the polymer. If the beads represent a group of monomers, one gains time because the number of variables decreases, but one loses the information contained in the left-out modes. With the current approach we keep all the degrees of freedom and thus do not lose information. Our simulation approach can also be combined with coarse-graining. In the Appendix we have worked out how to represent a group of two basepairs (a dimer) by one bead. It amounts to a well-defined shift to new parameters  $T_2^*$  and  $\nu_2$  for the dimerized chain such that it is equivalent to a dsDNA chain at full basepair resolution. The conversion factor  $c$  between the reduced time  $\tau$  and the real time  $t$  for a dimerized dsDNA chain is 8.5 times the value given in Eq. (45) for full basepair resolution. Thus, with the same time step in reduced time, the real time scale increases 8.5 times as fast; and there is the further natural gain of a factor 2 due to the reduction of the number of modes (i.e., degrees of freedom). Unfortunately however, for reasons that we do not understand yet, we find that  $\Delta\tau_{\max}$  for the dimerized dsDNA, determined numerically as described above, is smaller by a factor of 5 to 10 to that for a chain at full basepair resolution. Nevertheless, coarse-graining (dimerization) still allows for reaching longer times [and the properties  $Q(t)$  of a dimerized dsDNA chain correspond very well to those of a dsDNA chain at full basepair resolution], but primarily because of the reduction of the number of degrees of freedom.

Langevin dynamics simulations are widely used for the simulation of biopolymers, but most publications do not present a clear translation of the simulation time in real time (picoseconds or nanoseconds) and the experimental observation used to make this translation;

and certainly do not explore the maximal time step which does not cause significant systematic errors. We found reports of time steps of 12.9 ps [26], 5 ps [27] and 3.8 ps [28], in simulations in which a bead represents 4, 9 and 37 basepairs respectively; A back-of-the-envelope estimate then yields that by-and-large, these time steps, translated to full basepair resolution, are below the maximal time step estimated by us for an integration scheme in real-space coordinates.

Finally, the model also allows for adding forces to the monomers. In order to showcase this, we have simulated dsDNA segments in a shear flow, where the viscous drag force due to the shear flow makes the chain tumble in space. In the Supplementary Information we present a movie of a tumbling dsDNA chain of 255 basepairs at full resolution; the chain tumbles in water with a velocity field  $\mathbf{v}(\mathbf{r}) = \dot{\gamma}y\hat{x}$ , with shear rate  $\dot{\gamma} \approx 1.54 \times 10^8 \text{ s}^{-1}$  (which corresponds to Weissenberg number  $Wi \approx 5.55 \times 10^3$ , calculated from the moment of inertia of a straight rod of the same length as the dsDNA segment [23, 24]). In the movie the center of mass of the chain always remains at the origin of the co-ordinate system. The data for the movie are generated with  $\Delta\tau = \Delta\tau_{\text{max}} = 100$ , and took about three minutes to generate on a linux desktop; it contains 3,000 snapshots, with consecutive snapshots being 8 ns apart. A detailed study of the tumbling motion of the dsDNA in a shear flow is however not the focus of this paper; it will be taken up in an upcoming one.

## Acknowledgments

Ample computer time from the Dutch national cluster SARA is gratefully acknowledged.

## Appendix A: Dimerized dsDNA vs dsDNA at full basepair resolution

The parameters  $T^*$  and  $\nu$  are calculated by a fit to the force-extension curve for dsDNA as due to Wang *et al.* [2], which contains two dimensionless parameters: the ratio  $r$  of the persistence  $l_p$  to the monomer distance  $a$

$$r = \frac{l_p}{a}, \quad (\text{A1})$$

and the combination involving the force constant  $K_0$

$$y = \frac{K_0 l_p}{k_B T}. \quad (\text{A2})$$

For dsDNA one has  $r = 114$  and  $y = 12000$ . Then  $T^*$  and  $\nu$  follow from the relations [23]

$$T^* = \frac{(2r^2 + y)r}{y^2} \quad \text{and} \quad \nu = \frac{r^2}{2r^2 + y}. \quad (\text{A3})$$

If a bead represents a combination of two successive basepairs (a dimer), the distance between two consecutive dimers  $a_2 = 2a$ , implying that for the dimerized chain  $r_2 = r/2$ . The force constant  $K_0$  and the persistence length  $l_p$  remain the same for the dimerized chain, so  $y$  also remains the same. Then one can compute for the dimerized dsDNA chain  $T_2^*$  and  $\nu_2$  from the same equations (A3) with  $r$  replaced by  $r_2$ , which leads to the values  $T_2^* = 0.008$  and  $\nu_2 = 0.1875$ . These parameters guarantee that the force extension curve for the dimerized dsDNA chain is the same as that for a dsDNA chain at full basepair resolution.

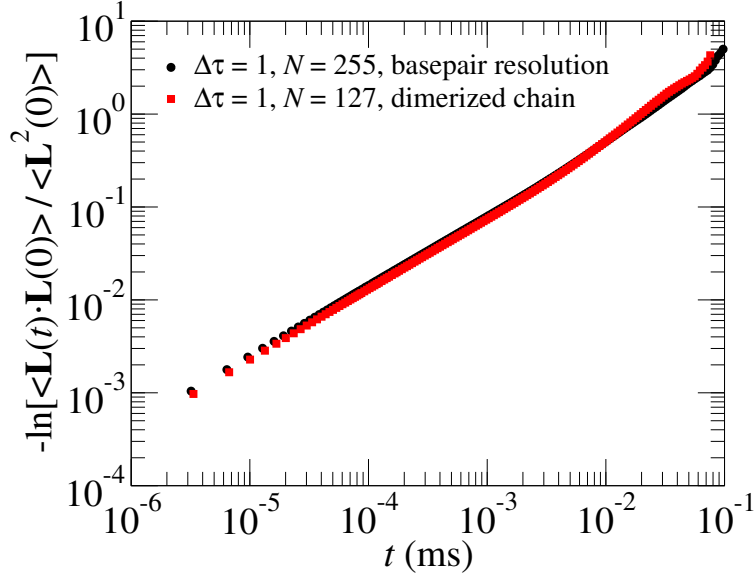


FIG. 5: The end-to-end vector data for a chain of 256 basepairs at full resolution, and that of the corresponding chain of 128 dimerized basepairs.

Using  $r_2$  in the equation for the time proportionality coefficient  $c$  in Eq. (43) and remembering that not only  $a$  doubles but also the friction constant  $\xi_2$  doubles to  $2\xi$ , we find for a dimerized dsDNA  $c_2 = 8.5c$ . I.e., a simulation with  $\Delta\tau$  for dimerized dsDNA yields the same curves as a simulation with  $8.5\Delta\tau$  for dsDNA full basepair resolution. As an illustration we have plotted in Fig. 5 the two curves for the end-to-end vector  $\mathbf{L}(t)$  in units in real times for dimerized dsDNA and the corresponding dsDNA at full basepair resolution.



How much this provides a gain in maximum time step must be found out by simulation of the dimerized chain with parameters  $T_2^*$  and  $\nu_2$ . For the various chain lengths that we have tried, it turns out that the  $\Delta\tau_{\max}$  values for a dimerized dsDNA chain are 5-10 times smaller than the  $\Delta\tau_{\max}$  values for the dsDNA chain at full basepair resolution. So the net gain of coarse graining is basically the speed-up due to the reduction in the number of modes.

- 
- [1] C. Bustamante, J. F. Marko, E. D. Siggia, and S. Smith, *Science* **265**, 1599 (1994); J. F. Marko and E. D. Siggia, *Macromolecules* **28**, 8759 (1995).
  - [2] M. D. Wang, H. Yin, R. Landick, J. Gelles and S. M. Block, *Biophys. J.* **72** 1335 (1997).
  - [3] A. Ott *et al.*, *Phys. Rev. E* **48**, 1642 (1993).
  - [4] F. Gittes, B. Mickey, J. Nettleton and J. Howard, *J. Cell Biol.* **120**, 923 (1993).
  - [5] O. Kratky and G. Porod, *Recl. Trav. Chim. Pays-Bas.* **68**, 1106 (1949).
  - [6] J. J. Hermans and R. Ullman, *Physica* **18**, 951 (1952).
  - [7] H. Daniels, *Proc. R. Soc. Edinburgh, Sect. A: Math. Phys. Sci.* **63**, 290 (1952).
  - [8] N. Saito, K. Takahashi and Y. Yunoki, *J. Phys. Soc. Jpn.* **22**, 219 (1967).
  - [9] H. Yamakawa, *Pure Appl. Chem.* **46**, 135 (1976).
  - [10] C. Bouchiat *et al.*, *Biophys. J.* **76**, 409 (1999).
  - [11] J. Wilhelm and E. Frey, *Phys. Rev. Lett.* **77**, 2581 (1996).
  - [12] J. Samuel and S. Sinha, *Phys. Rev. E* **66**, 050801 (2002).
  - [13] A. Dhar and D. Chaudhuri, *Phys. Rev. Lett.* **89**, 065502 (2002).
  - [14] P. Gutjahr, R. Lipowsky and J. Kierfeld, *Europhys. Lett.*, **76**, 994 (2006).
  - [15] B. Obermayer, O. Hallatschek, E. Frey and K. Kroy, *Eur. Phys. J. E* **23**, 375 (2007).
  - [16] R.E. Goldstein, S.A. Langer, *Phys. Rev. Lett.* **75**, 1094 (1995).
  - [17] N.-K. Lee, D. Thirumalai, *Biophys. J.* **86**, 2641 (2004).
  - [18] Y. Bohbot-Raviv, W. Z. Zhao, M. Feingold, C. H. Wiggins, R. Granek, *Phys. Rev. Lett.* **92**, 098101 (2004).
  - [19] T. B. Liverpool, *Phys. Rev. E* **72**, 021805 (2005).
  - [20] J. T. Bullerjahn, S. Sturm, L. Wolff and K. Kroy, *Europhys. Lett.* **96**, 48005 (2011).
  - [21] L. Harnau, R. G. Winkler and P. Reineker, *J. Chem. Phys.* **104**, 6355 (1996).
  - [22] R. G. Winkler, *J. Chem. Phys.* **118**, 2919 (2003).

- [23] G. T. Barkema and J. M. J. van Leeuwen, J. Stat. Mech. P12019 (2012).
- [24] G. T. Barkema, D. Panja and J. M. J. van Leeuwen, J. Stat. Mech. P11008 (2014).
- [25] P. E. Rouse, J. Chem. Phys. **21**, 1272 (1953).
- [26] C. Forrey and M. Muthukumar, Biophys. J. **91**, 25 (2006)
- [27] S. A. Allison, R. Austin, and M. Hogan, J. Chem. Phys. **90**, 3843 (1989).
- [28] G. Chirico and J. Langowski, Biopolymers **34**, 415 (1994).
- [29] N. C. Stellwagen, S. Magnúsdóttir, C. Gelfi, and P. G., Righetti, J. Mol. Biol. **305**, 1025 (2001).
- [30] E. Stellwagen and N. C. Stellwagen, Electrophoresis **23**, 2794 (2002).
- [31] W. Eimer and R. Pecora, J. Chem. Phys. **94**, 2324 (1991).
- [32] G. F. Bonifacio, T. Brown, G. L. Conn and A. N. Lane, Biophys. J. **73**, 1532 (1997).
- [33] G. L. Lukacs, P. Haggie, O. Seksek, D. Lechardeur, N. Freedman and A. S. Verkman, J. Biol. Chem. **275**, 1625 (2000).